JOURNAL OF MATERIALS SCIENCE **35** (2000) 427–435

Rubber toughening of plastics

Part XIII *Dilatational yielding in PA6.6/EPR blends*

C. B. BUCKNALL
Advanced Materials Department, Cranfield University, Bedford MK43 OAL, UK

A. LAZZERI
Centre for Materials Engineering, University of Pisa, Via Diotisalvi 2, Pisa 56100, Italy
E-mail: c.b.bucknall@cranfield.ac.uk

Tensile tests were carried out at both constant stress and constant extension rate on polyamide 6.6 blends containing 0–20 wt% of maleinated ethylene-propylene rubber (EPR-*g*-ma), using specimens conditioned at 50% RH. Longitudinal and lateral strain measurements on creep specimens showed that blends containing EPR-*g*-ma exhibited dilatation at tensile stresses above 27 MPa. This observation is consistent with the predictions of the particle cavitation model proposed in an earlier paper (A. Lazzeri and C. B. Bucknall, *J. Mater. Sci.* **28** (1993) 6799). In standard tensile tests on PA6.6/EPR-*g*-ma blends, cavitation preceded yielding (defined by the 1% offset strain). Creep and yield data obtained over a range of temperatures and strain rates were correlated using the Eyring equation. The onset of dilatation in these PA6.6/EPR blends was marked by a change in deformation kinetics, which is analysed using a modified version of Gurson's equation.

1. Introduction

A previous study on rubber-toughened nylons has shown that, in standard tensile tests, plastic dilatation begins at strains below 10%. Beyond this point, volume strain increases approximately linearly with extension [1]. Furthermore, in tensile creep experiments, the onset of dilatational yielding is accompanied by a rapid increase in deformation rate. This pattern of behaviour accounts qualitatively for the toughness of rubber-modified nylons in notched impact tests: controlled plastic dilatation accompanied by strain hardening in the matrix enables the material to overcome the constraints imposed by the notch on yielding.

A more quantitative approach to dilatational yielding in toughened plastics is developed in three recent papers [2–4]. This new theory, based on an energy-balance model, predicts that the onset of cavitation will occur at a critical volume strain, which is determined by the diameter of the rubber particles and the shear modulus of the rubber phase. The model also predicts that dilatational yielding will be concentrated into planar bands, formed at angles to the applied stress that are determined by the effective volume fraction of voids. The present paper examines the deformation and yield behaviour of a range of toughened nylon 6.6 blends in the light of this model.

2. Experimental

2.1. Materials

The PA6.6 was a commercial grade supplied by ICI. The rubber was a commercial ethylene-propylene copolymer (EPR) produced by Exxon, which was melt compounded with 1.5% maleic anhydride in the presence of 0.1% peroxide initiator, to form grafted functional groups. These anhydride groups were subsequently reacted with the terminal $-NH_2$ groups of the nylon in a second melt compounding operation. The resulting PA6.6 blends, containing 5, 10, 15 and 20 wt% of nylon-grafted EPR, were dried under vacuum for 16 h at 105°C, injection moulded into ASTM tensile bars [5], and conditioned for a minimum of 6 months at 20°C and 50% RH before testing. In this paper, the codes PA6.6/5 etc identify each blend by its EPR content in wt %. It should be noted that the volume fraction of rubber is substantially higher than the weight fraction because of density differences. Thus blend PA6.6/15 contains approximately 20 vol. % rubber.

Dynamic mechanical tests were carried out on the moisture-conditioned specimens at a frequency of 1 Hz. They showed an α relaxation peak at 25–30°C in both neat PA6.6 and PA6.6/EPR blends. For all materials, the water content reached a concentration of approximately 2.7% relative to the PA6.6 component. The creep and yield data presented below all refer to samples having this water content.

2.2. Methods

Tensile tests were carried out at temperatures between −40°C and 60°C, using an Instron tensometer, model 4302, equipped with an environmental chamber. Crosshead displacement rates were varied from 0.5 to 500 mm/min. Before testing, each specimen was held

in the chamber for a further 30 minutes after the chamber itself reached thermal equilibrium. Measurements of longitudinal strain and one lateral strain were made simultaneously, using two clip-on Instron extensometers.

Tensile creep measurements were made at 23°C, using the same Instron machine and extensometers. Loads were applied under computer control, in order to reach the required stress within 3 seconds. Dynamic mechanical tests were carried out between −100° and 150°C at a heating rate of 1 K min^{-1}, using a Polymer Laboratories DMTA machine, on specimens measuring $1 \times 12.8 \times 20$ mm which were cut from the central layer of each moulding to avoid skin effects.

Particle size distributions were determined by dissolving the nylon in formic acid, and subjecting the resulting suspension of rubber particles to sedimentation analysis using a Horiba particle analyser. Strained specimens from tensile bars were prepared in two ways for examination in the scanning electron microscope: (a) by microtoming thin sections parallel to the tensile draw direction; and (b) by cooling bars in liquid nitrogen, and fracturing on planes parallel to the draw direction. The fracture surfaces were coated with Au-Pd before examination.

3. Results

3.1. Tensile yielding at constant strain rate

Stress-strain curves for water-equilibrated PA6.6 blends containing 0, 10 and 20 wt% EPR-*g*-ma are compared in Fig. 1. The tests illustrated were conducted at −10°C, at a constant crosshead speed of 10 mm min^{-1}. The plain PA6.6 deforms relatively uniformly between 5 and 15% strain, then necks, and eventually breaks in the neck at a total extension of 25%. By contrast, the blend containing 20% EPR-*g*-ma breaks at an extension of 100% without necking. This blend begins to whiten throughout the gauge length at $\varepsilon \approx 5\%$, and draws uniformly up to the point of failure. Blends with lower rubber contents show intermediate behaviour, with a tendency to form a less pronounced neck than PA6.6, and to reach a higher elongation than the neat polymer before breaking.

Over the whole range of temperatures and strain rates tested, all tensile specimens initially show a lateral contraction that increases linearly with extension, and is typical of a viscoelastic material, reflecting the normal Poisson's ratio effect. However, at strains higher than 3%, some of the tensile bars undergo a more substantial decrease in cross-sectional area, involving localised neck formation.

Localised necking in PA6.6 is particularly associated with high stored energies in the specimen and loading system, and therefore with high yield stresses. Consequently, necking is most evident at low temperatures, high strain rates, and low rubber contents. High strain rates within the neck region generally result in heating, which is obvious to the touch. As noted by Cross and Haward [6], the sudden release of elastic energy from a long specimen into a region that is beginning to neck can generate sufficient local heating to raise the temperature by ∼25 K. In the present experiments, the observed levels of heating are more modest, but the net effect is the same: the temperature rises locally, thus ensuring that deformation continues through thinning and eventual failure of the existing neck region, rather than through neck propagation.

Until a neck begins to form, deformation within the parallel gauge region of the tensile bars is sufficiently uniform to allow the volume strain and true stress to be calculated with some confidence from longitudinal and lateral strain data. As lateral strains are measured along only one axis in the present experiments, it is necessary to assume that the deformation is transversely isotropic. Comparisons of lateral strain data, measured in the two orthogonal directions on 10 specimens, show that on average there is no more than 5% difference in magnitude between strains measured in the two directions.

Experiments on conditioned PA6.6 show no evidence of cavitation, in either scanning electron micrographs or volume strain measurements. Indeed, the density of PA6.6 actually increases on drawing, as noted in our earlier paper [1]. The conditions for tensile yielding in non-cavitating materials can conveniently be analysed using Considère's construction [7], in which true stress is plotted against extension ratio λ ($= L/L_0$), as shown in Fig. 2 for conditioned

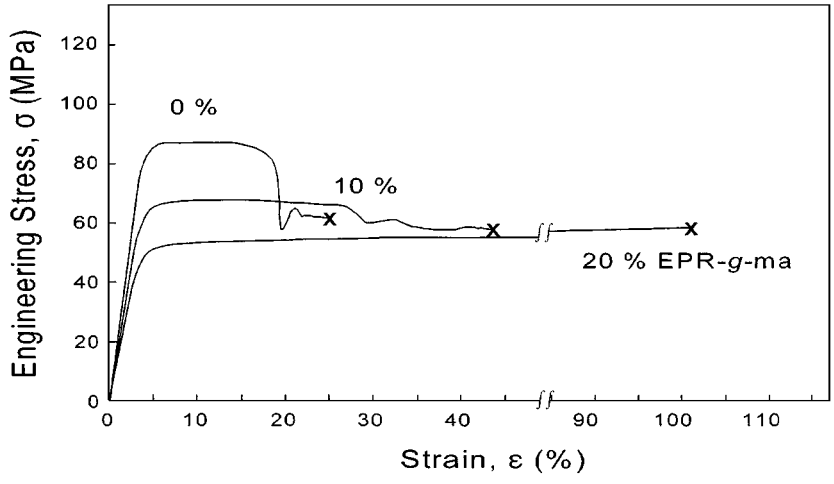

Figure 1 Engineering stress-strain curves obtained at −10°C for water-equilibrated PA6.6 containing 0, 10 and 20 wt% maleinated EPR.

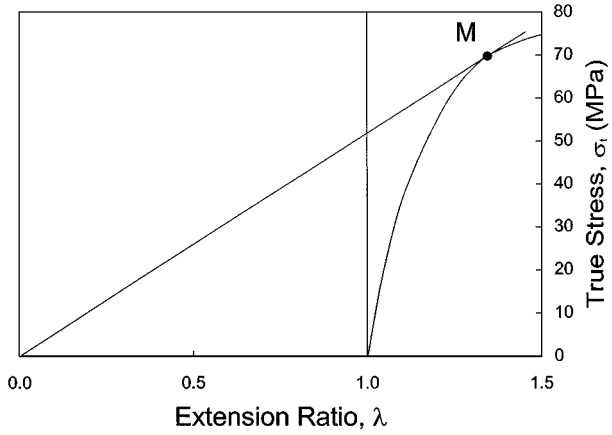

Figure 2 Considère construction for PA6.6, showing method for identifying the load maximum in tensile tests.

PA6.6/0. A tangent to the curve, drawn through the origin, marks the point at which tensile bars reach a load maximum. This construction explains why necking of PA6.6, accompained by a load drop, occurs at a strain $\varepsilon = (\lambda - 1) = 0.40$ when the temperature $T = 23^{\circ}\mathrm{C}$, and at $\varepsilon \sim 0.16$ when $T = -10^{\circ}\mathrm{C}$: not only are the stresses higher at $-10^{\circ}\mathrm{C}$, but also the shape of the true stress-extension curve changes over this temperature range.

Scanning electron microscopy reveals that rubber particles undergo cavitation within PA6.6 blends, which explains the observed whitening. The internal reduction in cross sectional area due to rubber particle cavitation occurs fairly uniformly throughout the parallel gauge section of the specimen, thereby drastically reducing the susceptibility of the blends to macroscopic necking. Strictly, Considère's treatment is not applicable in these cases, because the initiation of voids means that the material is no longer a continuum. A notional true stress can still be calculated from the applied load and the observed cross-sectional area, but this should not be regarded in the same way as a true stress for a continuum.

The increases with tensile strain in both volume strain and apparent true stress (neglecting internal cavitation) are illustrated in Fig. 3, for water-equilibrated PA6.6/15 at 23°C. The initial portion of the volume strain curve corresponds to the elastic response to be expected in a thermoplastic with a typical bulk modulus of 2.8 GPa. However, at a strain of about 8%, the curve turns upwards, indicating that cavitation is taking place in the blend. Electron microscopy shows that this cavitation is restricted to the rubber particles, and that no new internal surfaces are formed within the PA6.6 matrix itself [4]. In each of the PA6.6/EPR blends, the upturn in volume strain occurs at a true stress of between 30 and 35 MPa, which appears to correspond to the onset of cavitation in the rubber particles, a point that is discussed more fully later in this paper.

On unloading from a strain of 40%, specimens of both PA6.6 and its blends undergo substantial recovery over a period of 30 minutes, eventually reaching a strain of only 10%. On reloading, the previously-cavitated blend specimens show an immediate increase in volume strain, which is more rapid than on the first loading cycle. This observation confirms that plastic dilatation occurs readily once the rubber particles have cavitated, and that the initial resistance of the particles to void formation has an important influence upon subsequent deformation behaviour.

The tensile behaviour of the PA6.6/15 blend in the dry state is broadly similar to that of fully-conditioned material, but the dry blend is stiffer and requires higher true stresses to sustain cold-drawing. Consequently, it generates more cavitation, as shown in Fig. 4, giving a slope $\mathrm{d}V/\mathrm{d}\varepsilon$ of 0.33, as compared with 0.18 for the water-equilibrated material. The higher level and earlier onset of dilatation in the dry blend can be related directly to its higher modulus and yield stress. Because the material is subject to higher stresses, a larger fraction of the rubber particles reaches the critical strain for cavitation.

Tensile tests carried out over a range of conditions show that the yield behaviour of PA6.6 and its blends depends critically upon strain rate, temperature, and composition. As none of the materials tested exhibits a clearly-defined load maximum associated with the onset of plasticity, yield stresses σ_y are defined in terms of the 1% offset strain. Data for materials containing 0,

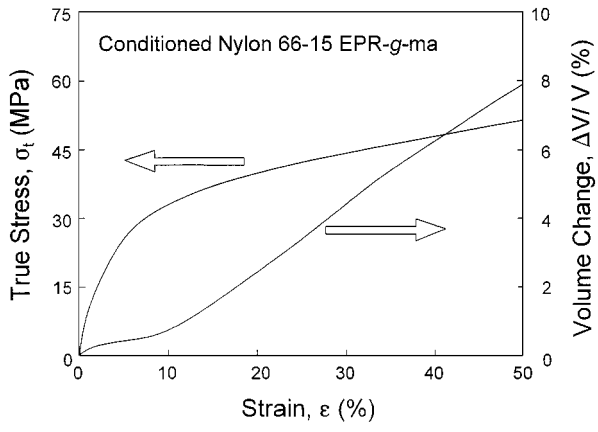

Figure 3 Dependence of true stress and volume upon elongation in water-equilibrated PA6.6/15 tested at 23°C, 10 mm min^{-1}.

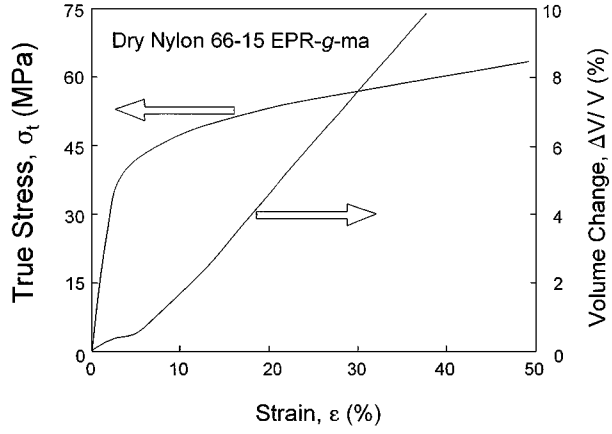

Figure 4 Dependence of true stress and volume upon elongation in dry PA6.6/15 tested at 23°C, 10 mm min^{-1}.

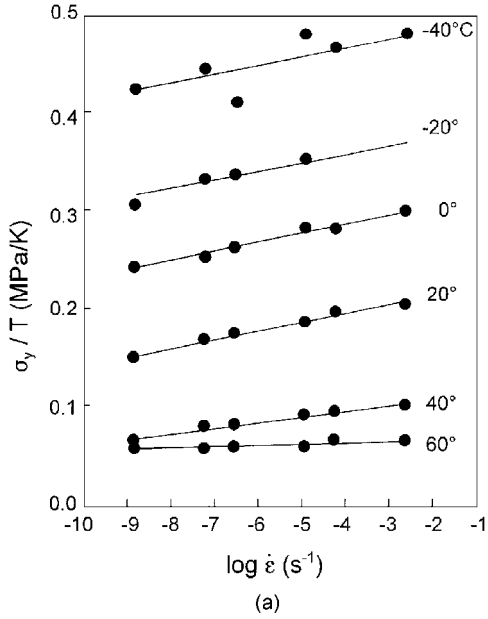

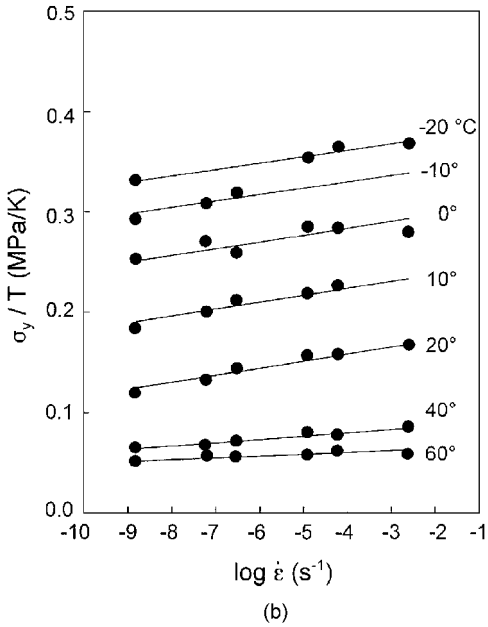

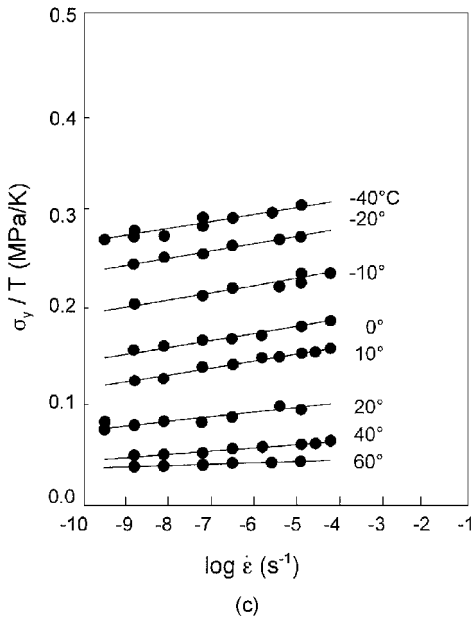

Figure 5 Eyring curves of σ_y/T against $\log\dot{\varepsilon}$ for water-equilibrated PA6.6 containing (a) 0%; (b) 10 wt % and (c) 20 wt % EPR-*g*-ma.

10 and 20 wt % EPR are summarised in Fig. 5. They show that yielding follows the Eyring equation [7, 8]:

$$\frac{\sigma_y}{T} = \frac{1}{\gamma V^*}\left[\frac{\Delta H}{T} + R\ln\left(\frac{\dot{\varepsilon}_y}{\dot{\varepsilon}_0}\right)\right] \qquad (1)$$

where γ is a scalar stress concentration factor, relating the local stress on the flow element to the nominal applied stress; V^* is the activation volume for the flow process, ΔH is the activation enthalpy, and $\dot{\varepsilon}_y$, $\dot{\varepsilon}_0$ are current and reference strain rates.

At temperatures up to 20°C, the Eyring plots give a set of parallel straight lines for each material tested, suggesting that a single deformation process dominates yielding. Above 20°C, which is approximately the glass transition temperature of the water-equilibrated PA6.6, the slopes of the lines decrease and the activation volume for the rate-determining step in the yield mechanism increases from 1.1 nm^3 at 20°C to 5.4 nm^3 at 60°C.

By comparing Fig. 5a, b and c, it can be seen that the sets of parallel lines define a slope $[\partial(\sigma/T)/\partial\log\dot{\varepsilon}]$ that decreases with increasing rubber content. The obvious explanation for this trend is that the low-modulus rubber particles support only a small fraction of the stress applied to the specimen at the load maximum, so that the local stress on the deforming PA6.6 phase becomes progressively higher as rubber is added to the blends. Stress concentration factors and activation energies for all five materials are presented in Table I. The value of γ increases sharply between 0 and 5% rubber, then rises more gradually. The rapid initial increase in γ reflects a change in deformation mechanism, from yielding without cavitation in PA6.6/0 to dilatational yielding in PA6.6/5. The activation energy ΔH shows no systematic trend, suggesting that the observed variations are due to experimental scatter.

3.2. Creep

The creep behaviour of water-equilibrated PA6.6 and of a PA6.6 blend containing 20 wt% EPR-*g*-ma was discussed in the previous paper [1]. For both materials, data on creep strain $\varepsilon(t)$ at time t can be fitted to the Andrade equation [9]:

$$\varepsilon(t) = \varepsilon(0) + bt^{1/3} \qquad (2)$$

In the present paper, the main reason for introducing Equation 2 is to define the parameter b, which is essentially a rate coefficient [1] similar to those used in

TABLE I Activation volumes and stress concentration factors for water-equilibrated PA6.6 blends

Rubber content (%)	γV^* (nm^3)	γ	ΔH (kJ/mol)
0	1.13	1	205
5	1.62	1.43	227
10	1.87	1.65	218
15	2.03	1.80	201
20	2.03	1.79	184

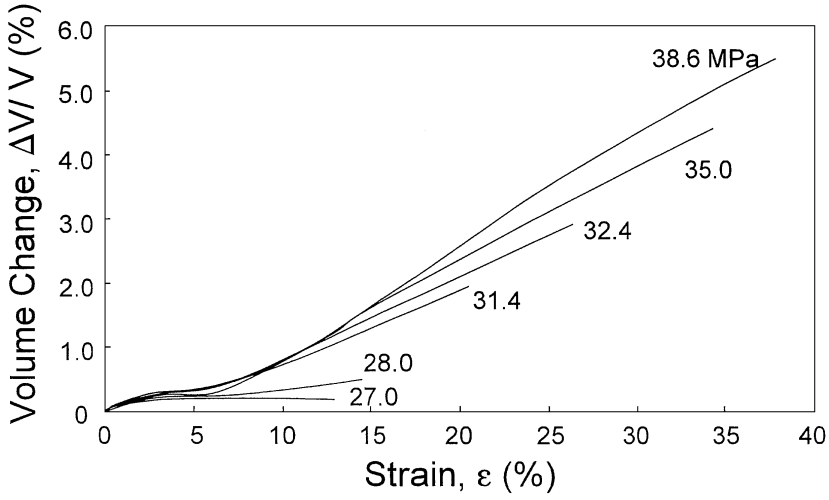

Figure 6 Effects of applied stress on dilatation in water-equilibrated PA6.6/15 creep specimens at 23°C.

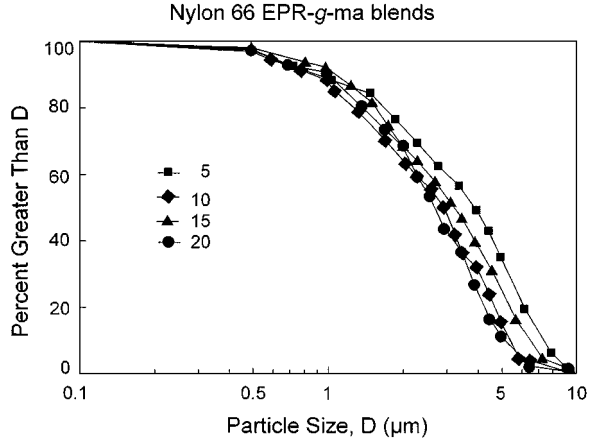

Figure 7 Distributions of rubber particle size in PA6.6/EPR blends.

chemical kinetics. For PA6.6, plots of log b against applied stress σ_{appl} gave a linear relationship, in accordance with the Eyring equation. In the case of the PA6.6/20 blend, a similar straight line was obtained for stresses up to about 30 MPa, above which there was an abrupt increase in slope as the data followed another linear relationship [1]. Significantly, this transition in creep behaviour coincided with the onset of dilatational deformation.

In creep experiments, the PA6.6/15 blend shows a pattern of behaviour similar to that of the 20 wt % EPR blend. The creep strain $\varepsilon(t)$ increases linearly with $t^{1/3}$, and plots of log b against σ give two straight lines intersecting at $\sigma = 27$ MPa. Data on volume changes $\Delta V/V$ during creep tests on PA6.6/15 are presented in Fig. 6. They show that there is a transition in behaviour with increasing stress, from creep at constant volume to pronounced dilatational deformation. The first indications of this change occur at $\sigma_{crit} = 28$ MPa. Noting that an applied tensile stress of 27 MPa corresponds to a mean normal stress σ_m of 9 MPa, and taking the bulk modulus of moisture-equilibrated PA6.6 as 2800 MPa, the critical elastic volume strain for cavitation obtained from this experiment is approximately 0.32%.

3.3. Particle size distribution and morphology

Sedimentation data from the Horiba equipment are obtained in the form of histograms showing the volume fraction of particles in each of the selected size ranges. These data have been used to generate curves of cumulative volume fraction against particle diameter, which are presented in Fig. 7. As expected in a blend made by melt compounding, the particle size distributions are relatively broad.

Scanning electron microscopy of microtomed and etched surfaces shows that most of the particles are roughly spherical, although some are more irregular in shape. Transmission electron microscopy of ultrathin sections reveals that some PA6.6 sub-inclusions are present within the EPR phase. Similar observations have been reported by Ban *et al*. [10].

4. Discussion

This work has shown that added rubber particles not only reduce the yield stress (a result that can be achieved equally well by raising the temperature), but also affect the deformation behaviour of nylon 6.6 in a number of other ways. When the applied stresses are high enough, the rubber particles undergo cavitation, thereby promoting dilatational shear yielding in the matrix [2, 4]. Both rubber particle cavitation and matrix shear deformation play an important part in the extension and failure behaviour of PA6.6-EPR blends under uniaxial tension. In standard tensile tests on these materials, dilatational yielding enables the parallel gauge portion to draw uniformly, without the necking that is characteristic of PA6.6 itself. Eyring plots of tensile creep data show that rubber particle cavitation allows the PA6.6/15 blend to deform at much higher rates than would otherwise be observed over the same range of applied stresses [1]. The energy-balance model for cavitation, in combination with theories of dilatational yielding [2–4], provides a quantitative basis for analysing the complex responses of rubber particles to applied stress, and the cavitation diagrams introduced in previous papers

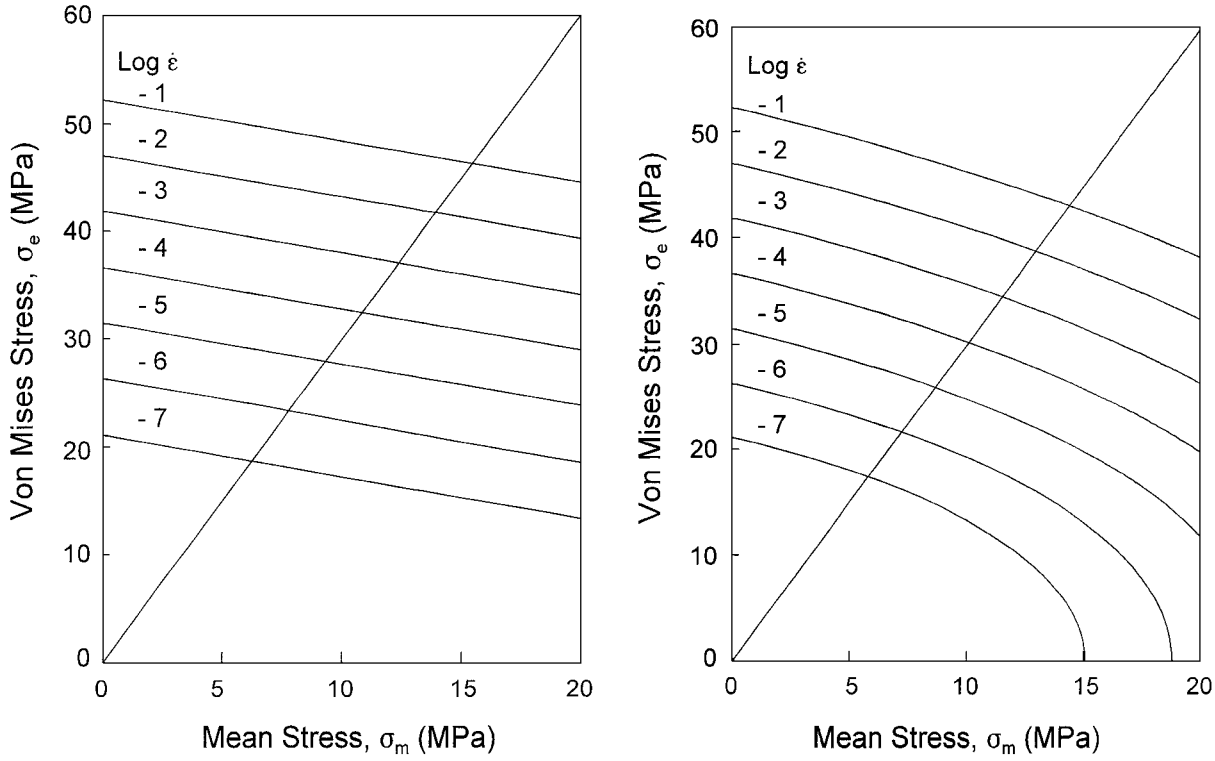

Figure 8 Yield envelopes at 23°C over a range of strain rates for water-equilibrated PA6.6/15 (containing 20 vol. % rubber) calculated from tensile yield data: (a) with no cavitation; (b) with full cavitation of the rubber particles. Construction line through origin defines uniaxial tension.

[2, 4] offer a convenient method of visualising these responses.

4.1. Cavitation diagrams

Cavitation diagrams were developed in order to show graphically how the criteria for cavitation of rubber particles compare with the yield and fracture behaviour of toughened plastics [2, 4]. The principles underlying this approach are illustrated in Figs 8 and 9. The ordinate is the (von Mises) effective stress σ_c and the abscissa is the mean normal stress σ_m. In this co-ordinate frame, a line of slope 3 defines a state of uniaxial tension.

For plain nylon, containing neither rubber particles nor voids, yield envelopes are represented in this $\sigma_e - \sigma_m$ stress space by straight lines, which are generators of right circular cones in principal (Westergaard) stress space [4]. For purposes of illustration, the pressure coefficient μ for PA6.6 is here taken as 0.39. In polymers, the strong dependence of yield stress upon strain rate means that there is no unique yield envelope, even at a single fixed temperature. Instead, yield is represented by a series of parallel lines, each corresponding to a different strain rate, as illustrated in Fig. 8a for a blend containing 20 vol% (15 wt%) of EPR. The calculations used in preparing this diagram are based on Eyring plots of yield stress data similar to those shown in Fig. 5a. Because of these strain rate effects, the region below a given yield envelope cannot strictly be regarded as representing purely elastic behaviour in the material, as it would in a metal. There is always some time-dependent deformation, albeit very slow, even at low stresses.

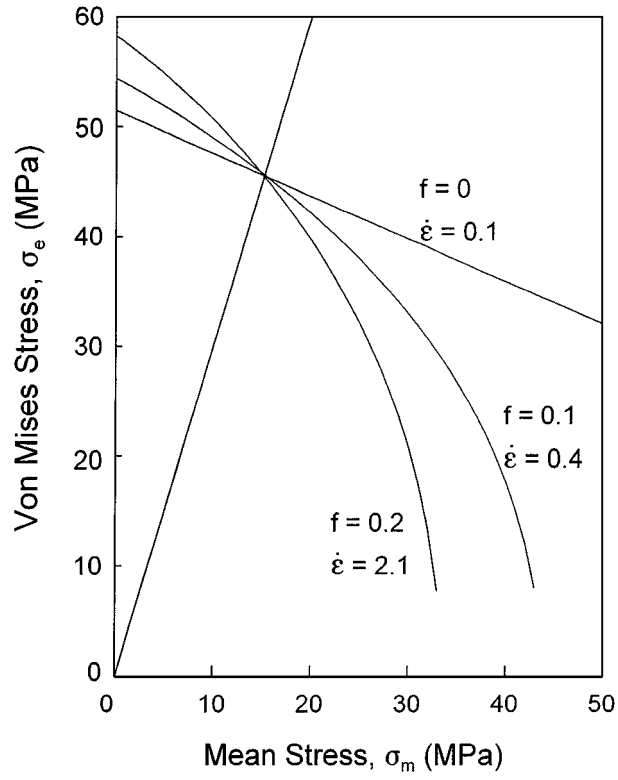

Figure 9 Diagram showing that rubber particle cavitation produces a marked acceleration in strain rate at fixed applied stress. Curves intersect under conditions of uniaxial tension. Curves obtained from data shown in Figs 5 and 8 (see text).

The yield behaviour changes when the rubber particles cavitate. Fig. 8b shows a series of yield envelopes for the same toughened nylon as in Fig. 8a, over the same range of strain rates. The curves were obtained

using a modified version of Gurson's equation for plastic flow in porous ductile media [11]. For a cavitating polymer, it is necessary to include in the equation a term in μ, the pressure coefficient of yielding, as well as terms in f, the volume fraction of voids [2, 4]. The resulting equation is [2, 12, 13]:

$$\frac{\sigma_e^2}{\sigma_0^2} = \left(1 - \frac{\mu\sigma_m}{\sigma_0}\right)^2 - 2fq_1\cosh\left(\frac{3q_2\sigma_m}{2\sigma_0}\right) + (q_1 f)^2 \quad (3)$$

where σ_0 is the effective stress at yield when the mean normal stress σ_m and the void content f are both zero. The factors q_1 and q_2 were introduced originally by Tvergaard to improve the fit between Gurson's predictions and data from experiment and numerical analysis in studies on metals [14, 15]; they were later applied to polymers [12, 13]. In the present analysis, the values used are $q_1 = 1.375$ and $q_2 = 0.927$ [12]. Typical calculated values of q_1 and q_2 are between 1.1 and 1.5.

When $\sigma_m = 0$, rubber particles have the same effect upon yield stress as voids have. Consequently, Equation 3 can be used to calculate $\sigma_0(\phi)$, the yield stress, measured at $\sigma_m = 0$, for a rubber-toughened polymer containing a volume fraction ϕ of intact (void-free) rubber particles. The first step is to set $\sigma_m = 0$, $f = \phi$, and $\sigma_0 = \sigma_0(0)$, where $\sigma_0(0)$ is the yield stress of the unmodified nylon matrix at the chosen temperature and strain rate. The yield stress σ_e calculated in this way is then equal to $\sigma_0(\phi)$. For nylon blends with $\phi = 0.2$, values of $\sigma_0(\phi)$ at 23°C over a range of strain rates can then be obtained directly from the intercepts with the ordinate in Fig. 8a.

In the more general case, a toughened polymer with a total rubber volume fraction of Φ will contain a combination of intact particles, of volume fraction ϕ, and cavitated particles, initially occupying volume fraction f, where $\Phi = (\phi + f)$. In other words, for the purposes of the present discussion, cavitated rubber particles will be treated as equivalent to voids of the same size and volume, provided that the particles have not expanded as a result of matrix yielding. This is a reasonable assumption for nylon-EPR blends, but cannot be applied to all rubber-toughened blends, because some types of rubber particles are capable of supporting significant stresses even after cavitation.

It follows that $\sigma_e(\phi, f)$ can be calculated using Equation 3 by setting $\sigma_0 = \sigma_0(\phi)$ and inserting the relevant value of f. This procedure was used to generate the curves shown in Fig. 8b, with $\phi = 0$ and $f = 0.2$. In compression, where any voids that might be present will close up, and at $\sigma_m = 0$, the yield envelopes for intact and cavitated particles are indistinguishable. However, under tensile mean stress the two sets of curves diverge. Instead of the right circular cones generated by the Drucker-Prager (pressure-modified von Mises) criterion (Fig. 8a), envelopes for cavitated materials are round-ended cones in principal stress space [4].

These principles were used to generate yield envelopes at 23°C for PA6.6 blends containing 20 vol. % rubber, with different combinations of ϕ and f. The results are presented in Fig. 9. They illustrate a very important principle relating to polymers capable of cavitating, namely that the strain rate resulting from the application of a given stress does not have a unique value, but varies substantially with the extent of cavitation. The three curves shown in Fig. 9 were all calculated for a polymer containing 20 vol.% of rubber particles, and are based on experimental data from the present programme. If none of the particles has cavitated ($f = 0$) the strain rate $\dot{\varepsilon}$ is 0.1 s^{-1}. If 50% of the particles have cavitated ($f = 0.1$), $\dot{\varepsilon}$ increases to 0.4 s^{-1}, and if all of the particles have cavitated ($f = 0.2$) the strain rate reaches its maximum attainable value of 2.1 s^{-1}. The three curves intersect where they cross the construction line for uniaxial tension.

As mentioned earlier, the main purpose in constructing a cavitation diagram is to compare the various yield envelopes with criteria for cavitation, which occurs at a critical volume strain (or, equivalently, a critical mean stress σ_m). For materials containing a distribution of particle sizes, there is a corresponding range of critical mean stresses, which can be represented by a cavitation zone, as illustrated in Fig. 10. Cavitation begins in the larger particles, on the low-stress side of this zone, and proceeds to affect smaller particles as the applied stress increases. The cavitation zone shown in Fig. 10 was calculated on the basis of particle size data from Fig. 7, using the energy-balance model described in earlier papers [2–4]. Two cases are considered. Fig. 10a shows yielding under uniaxial tension, at low strain rate and a stress of 27 MPa, which is below the level at which the rubber particles will cavitate; while Fig. 10b shows the contrasting case, with yielding at a higher strain rate and a tensile stress of 40 MPa, where virtually all of the particles have cavitated, and yielding follows Equation 3 with $f = 0.2$. In the absence of cavitation, an applied stress of 40 MPa would give a substantially reduced strain rate, amounting to less than 10% of that for the fully-cavitated nylon blend.

Yield stress data obtained over a range of strain rates at 20°C are plotted in Fig. 11 for the PA6.6/15 blend, which contains 20 vol. % rubber. They show that yielding occurs at stresses between the upper bound line, corresponding to $f = 0$, and the lower bound at $f = 0.2$. The points appear to move towards the lower bound curve as the yield stress increases with strain rate, a result that supports the theoretical prediction that the fraction of particles cavitated increases with strain rate.

4.2. Interpretation of tensile data

The above analysis provides considerable insight into the deformation behaviour of toughened PA6.6 in uniaxial tension. It is clear both from creep data and from theoretical considerations that the rubber particles in the present series of blends initially cavitate at a mean stress in the range 9–12 MPa. At room temperature, thermal contraction stresses appear to play only a minor part in the process, essentially because the water-equilibrated matrix is close to its glass transition temperature, where the rubber particles can be considered to be in mechanical equilibrium with the matrix. The main driving force for cavitation is therefore the mechanical loading on the specimen. A significant fraction of the energy for rubber

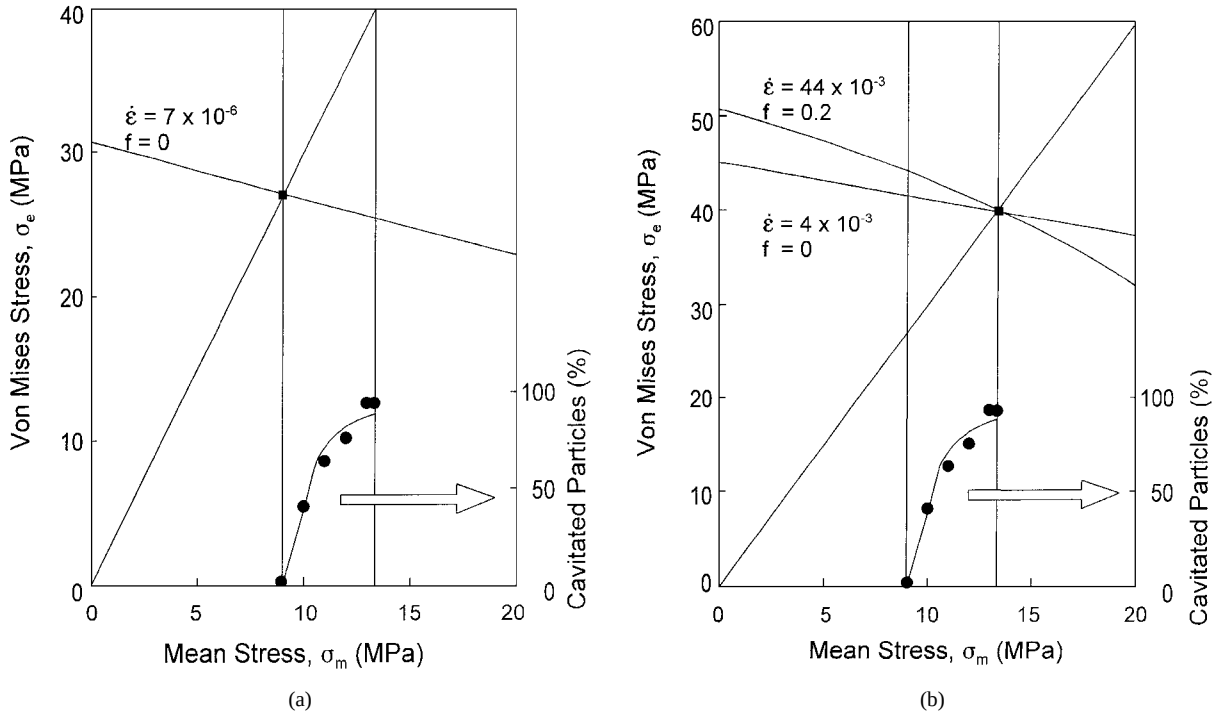

Figure 10 Cavitation diagram showing effect of increasing tensile creep stress from (a) 27 MPa, below the critical stress for the rubber particles in the present study; to (b) 40 MPa, where extensive particle cavitation has taken place ($f \approx 0.2$). Without cavitation, creep at 40 MPa is much slower.

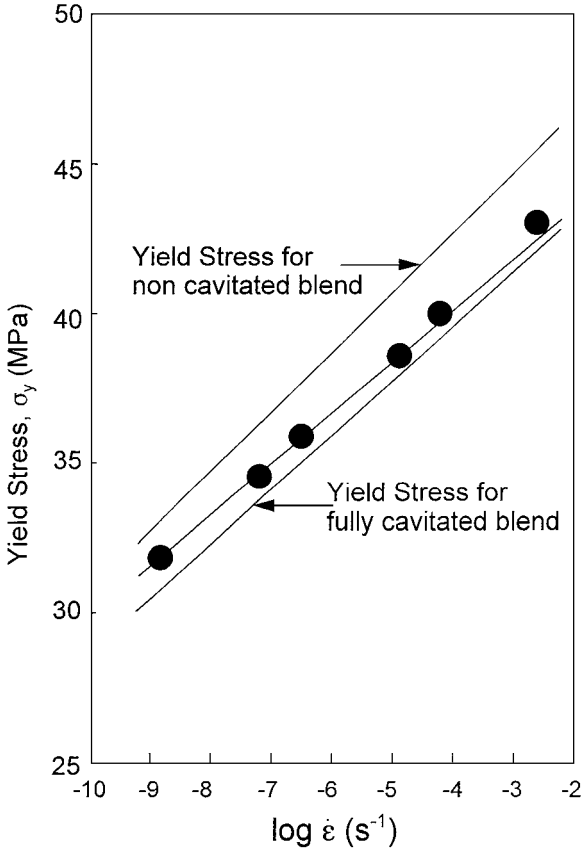

Figure 11 Tensile yield stress data over a range of strain rates at 20°C for the PA6.6/15 blend, which contains 20 vol. % rubber. The upper and lower lines respectively define the maximum and minimum yield stress envelopes, without cavitation and with full cavitation.

particle cavitation comes from the surrounding matrix, and the energy-balance theory therefore predicts that the critical volume strain for cavitation will increase with increasing rubber content, as the volume fraction of matrix falls, and the mechanical constraints that it imposes on the particles decrease. Another factor affecting dilatational yielding in the present study is that the rubber particles produced using melt compounding decrease in size with increasing rubber content, again making the particles harder to cavitate at higher concentrations.

The foregoing discussion based on cavitation diagrams provides a clear quantitative explanation for the increase in creep rate (over and above that obtained by extrapolating Eyring rate data) that is observed at stresses above the critical mean stress for rubber particle cavitation ($\sigma_m \approx 9$ MPa). Tensile tests on PA6.6 blends often reach stresses much higher than 27 MPa, and it is clear from the resulting data that most of the specimens tested have cavitated at stresses well below the yield point defined by the 1% offset strain. Thus in Fig. 5b a single deformation mechanism controls yielding in blend PA6.6/10 over the range $-20°$ to 20°C, where in all cases $\sigma_y > 27$ MPa. Only at $T \geq 40$°C do the yield stresses for this blend become low enough to permit significant plastic deformation without cavitation. Consequently, yield stress data for temperatures below 40°C form a coherent set of parallel straight lines. A similar set of straight lines is obtained for the PA6.6/20 blend between $-40°$ and 10°C, as shown in Fig. 5c. In this material, yield data obtained at 20°C are within the 27–30 MPa band, where cavitation effects are minimal, and the slope $[\partial(\sigma_y/T)/\partial \ln \dot{\varepsilon}]_T$ decreases.

Even at high temperatures, where yielding occurs before the conditions necessary for rubber particle cavitation are satisfied, it is still possible for dilatational yielding to contribute to the overall deformation of PA6.6/rubber blends, because tensile stresses continue to rise beyond the yield point, as a result of strain hardening. In tensile tests at constant strain rate, the only

conditions under which no volume increase was observed were for PA6.6/20 blends tested at 60°C.

5. Conclusions

This work on water-equilibrated toughened PA6.6 has shown that cavitation occurs at tensile stresses above 27–30 MPa, which correspond to mean stresses (negative pressures) of 9–10 MPa. These figures are consistent with the model proposed in our previous papers [2–4], which relates cavitation of the rubber to the volumetric strain energy stored within the individual particles and their associated shells of rigid matrix. Observed values of critical volume strain at cavitation ($\Delta V \sim 0.33\%$) are in satisfactory agreement with the predictions of the model. Furthermore, the formation of angled dilatational bands, also predicted by the model, has been confirmed using electron microscopy [4].

Dilatation is not observed in unmodified PA 6.6. It is also not seen in rubber-toughened PA6.6 above about 40°C, because yield stresses then fall below 30 MPa. When dilatation effects are very small, or absent, tensile specimens of nylon undergo necking on reaching strains of ∼40%. By contrast, toughened nylons generally exhibit significant dilatation in standard tensile tests, undergoing uniform drawing to very high strains; external cross-sectional areas decrease relatively little, because necking occurs internally.

The Eyring equation provides a satisfactory basis for correlating the yield behaviour of toughened and untoughened nylons, as defined by the 1% offset yield stress, over a range of strain rates and temperatures. For tests carried out below the T_g of the nylon matrix, apparent activation volumes V^*_{app} are independent of temperature, but increase with rubber content, from 1.1 to 2.0 nm^3. Calculated activation energies for yielding are in the range 180–230 kJ/mol, showing no clear trend with rubber content.

By combining the theoretically-based cavitation model with experimental data on the strain rate- and temperature-dependence of yield stress, it is possible to gain an insight into the factors controlling deformation micro-mechanisms in rubber-toughened PA 6.6. According to the model, cavitation occurs when the volume strain in the rubber particles reaches a critical value. At the same time, applied strain rate and temperature act independently in controlling the stress and strain at yield in the matrix. Thus shifts in cavitation behaviour due to changes in particle size, and changes in matrix yield characteristics as a result of either water uptake or variations in test conditions, determine whether the material shows a significant amount of dilatational yielding before final fracture. This is especially important in impact tests on sharply-notched specimens, where cavitation of the rubber particles plays an essential part in obtaining successful toughening.

Acknowledgements

The authors thank ICI Wilton Research Centre, the Science and Engineering Research Council of the UK (GRH 06354), and MURST of Italy for their support of this project.

References

1. C. B. BUCKNALL, P. S. HEATHER and A. LAZZERI, *J. Mater. Sci.* **24** (1989) 2255.
2. A. LAZZERI and C. B. BUCKNALL, *ibid.* **28** (1993) 6799.
3. C. B. BUCKNALL, A. KARPODINIS and X. C. ZHANG, *ibid.* **29** (1994) 3377.
4. A. LAZZERI and C. B. BUCKNALL, *Polymer* **36** (1995) 2895.
5. ASTM Standard D 638.
6. A. CROSS and R. N. HAWARD, *J. Polym. Sci., Polym Phys edn* **11** (1973) 2423.
7. N. G. McCRUM, C. P. BUCKLEY and C. B. BUCKNALL, "Principles of Polymer Engineering," 2nd edn (Oxford University Press, Oxford, 1997).
8. H. EYRING, *J. Chem. Phys.* **4** (1936) 283.
9. E. N. da C. ANDRADE, *Proc. Roy. Soc.* **A84** (1910) 1.
10. L. L. BAN, M. J. DOYLE, M. M. DISKO and G. R. SMITH, *Polymer Comm.* **29** (1988) 163.
11. A. L. GURSON, *J. Engng. Mater. Technol., Trans. ASME* **99** (1977) 2.
12. H. J. JEONG and J. PAN, *Int. J. Solid Structures* **32** (1995) 3669.
13. A. C. STEENBRINK, E. VAN DER GIESSEN and P. D. WU, *J. Mech. Phys Solids* **45** (1997) 405.
14. V. TVERGAARD, *Int. J. Fracture*, **17** (1981) 389.
15. *Idem., ibid.* **18** (1982) 237.
16. C. CHENG, A. HILTNER, E. BAER, P. R. SOSKEY and S. G. MYLONAKIS, *J. Appl. Polym. Sci.* **52** (1994) 177.

Received 6 March 1998
and accepted 22 July 1999